JACS
JOURNAL OF THE AMERICAN CHEMICAL SOCIETY
Article
pubs.acs.org/JACS

Doped Semimetal Clusters: Ternary, Intermetalloid Anions $[Ln@Sn_7Bi_7]^{4-}$ and $[Ln@Sn_4Bi_9]^{4-}$ (Ln = La, Ce) with Adjustable Magnetic Properties

Felicitas Lips,[†] Małgorzata Hołyńska,[†] Rodolphe Clérac,[‡,¶] Uwe Linne,[†] Inga Schellenberg,[§] Rainer Pöttgen,[§] Florian Weigend,[⊥] and Stefanie Dehnen*,[†]

[†]Fachbereich Chemie and Wissenschaftliches Zentrum für Materialwissenschaften, Philipps-Universität Marburg, Hans-Meerwein-Straße, D-35032 Marburg, Germany

[‡]CNRS, CRPP, UPR 8641, Centre de Recherche Paul Pascal, Equipe "Matériaux Moléculaires Magnétiques", 115 avenue du Dr. Albert Schweitzer, F-33600 Pessac, France

[¶]Univ. Bordeaux, CRPP, UPR 8641, F-33600 Pessac, France

[§]Institut für Anorganische und Analytische Chemie, Westfälische Wilhelms-Universität Münster, Corrensstrasse 30, D-48149 Münster, Germany

[⊥]Karlsruher Institut für Technologie (KIT), Institut für Nanotechnologie, Hermann-von-Helmholtz-Platz 1, D-76344 Eggenstein-Leopoldshafen, Germany

Supporting Information

ABSTRACT: Two K([2.2.2]crypt) salts of lanthanide-doped semimetal clusters were prepared, both of which contain at the same time two types of ternary intermetalloid anions, $[Ln@Sn_7Bi_7]^{4-}$ and $[Ln@Sn_4Bi_9]^{4-}$, in 0.70:0.30 (Ln = La) or 0.39:0.61 (Ln = Ce) ratios. The cluster shells represent nondeltahedral, fullerane-type arrangements of 14 or 13 main group metal atoms that embed the Ln^{3+} cations. The assignment of formal +III oxidation states for the Ln sites was confirmed by means of magnetic measurements that reveal a diamagnetic La(III) compound and a paramagnetic Ce(III) analogue. Whereas the cluster anions with a 14-atomic main-group metal cage represent the second examples in addition to a related Eu(II) cluster published just recently, the 13-atomic cages exhibit a yet unprecedented enneahedral topology. In contrast to the larger cages, which accord to the Zintl–Klemm–Busmann electron number–structure correlation, the smaller clusters require a more profound interpretation of the bonding situation. Quantum chemical investigations served to shed light on these unusual complexes and showed significant narrowing of the HOMO–LUMO gap upon incorporation of Ce^{3+} within the semimetal cages.

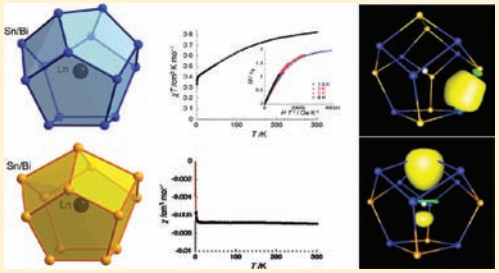

INTRODUCTION

Metal doping has been widely applied in materials chemistry in order to achieve influences or provoke additional characteristics such as electronic, optical, or magnetic properties, with n-/p-type doping by electron-donor or -acceptor impurities in semiconductors as the classical example.

In the recent past, the concept of metal doping has also been discussed for molecular compounds, in so-called endohedral clusters, such as metallofullerenes.[1] Alkali metals as well as lanthanide ions inserted into the crystal structure or encapsulated inside carbon cages, respectively, caused significant changes in chemical and physical properties, such as metallic or superconducting characteristics for solid state M_xC_{60} (M = K, x = 3)[2] and different magnetic properties for $Ln@C_{82}$ (Ln = La, Eu, Gd), upon variation of the interstitial lanthanide ion.[1]

Intermetalloid endohedral clusters[3] contain interstitial metal atom(s) within main-group (semi)metal cages. For this reason, these clusters were also discussed as models for doped materials.[4] In addition to its impact on physical properties, the incorporation of transition metal atoms in main-group metal cages serves to stabilize cluster shells $[E_n]^{q-}$ (n = 10, 12, 17, 18, 20; q = 2–4), most of which have not been observed as empty entities so far.[5] A limited number of amazing clusters were generated as polyhedra, encapsulating one atom, as in $[Ir@Sn_{12}]^{3-}$ [6] and $[M@Pb_{12}]^{2-}$ (M = Ni, Pd, Pt),[7] two atoms as in $[Pd_2@E_{18}]^{4-}$ (E = Ge, Sn)[8] and a unique example with three atoms in $[Ni–Ni–Ni@(Ge_9)_2]^{4-}$.[9] Thus, clusters with more than 12 atoms were only isolated with two or three interstitial transition metal atoms, whereas for a single encapsulated atom, the observation of cages with more than 12 vertices has been restricted to gas-phase species so far.[10] Some main-group atom cages with lanthanide ions have been investigated by photoelectron spectroscopy and quantum chemical investigations.[11] This way, several 14- or 13-atomic

Received: September 30, 2011
Published: November 23, 2011

   dx.doi.org/10.1021/ja209226b | J. Am. Chem.Soc. 2012, 134, 1181–1191

Table 1. EDX Analyses of 1 and 2 (Sn, Bi, K, La, or Ce, respectively)

compound	element	*k*-ratio	ZAF	atom %	atomic ratio observed (calc.)	element wt %	wt % err. ($1-\sigma$)
1	K-K	0.0569	1.094	21.9	4.0	6.2	±0.3
	Sn-L	0.2397	1.237	34.4	6.3	29.7	±0.9
	Bi-M	0.5648	1.056	39.3	7.2	59.6	±0.9
	La-L	0.0369	1.213	4.4	0.8	4.5	±0.5
	total			100	18.3	100	
2	K-K	0.0444	1.409	22.5	4.0	6.3	±0.2
	Sn-L	0.1658	1.450	28.6	5.1	24.1	±0.7
	Bi-M	0.6039	1.059	43.1	7.7	63.9	±0.9
	Ce-L	0.0445	1.294	5.8	1.0	5.8	±0.7
	total			100	17.8	100	

Table 2. X-ray Measurement, Structure Solution and Refinement Data of 1 and 2

compound	1	2
empirical formula	$C_{73.40}H_{149.6}Bi_{7.6}K_4La_1N_{9.4}O_{24}Sn_{6.1}$	$C_{73.40}H_{145.50}Bi_{8.22}Ce_1K_4N_{9.40}O_{24}Sn_{5.17}$
formula weight/g·mol^{-1}	4155.59	4171.85
crystal color, shape	black rhombus-like plate	black rhombus-like plate
crystal size/mm^3	0.18 × 0.15 × 0.06	0.21 × 0.06 × 0.03
crystal system	monoclinic	monoclinic
space group	$P2_1/c$	$P2_1/c$
a /Å	28.476(6)	28.489(6)
b /Å	16.345(3)	16.305(3)
c /Å	29.076(6)	29.025(6)
β /deg	117.13(3)	118.34(3)
V /Å^3	12044(4)	11867(4)
Z	4	4
ρ_{calc} /g·cm^{-3}	2.29	2.34
μ(Mo Kα) /mm^{-1}	12.8	13.8
2θ range /deg	2.80−50.00	2.96−50.00
reflns. measured	76768	72645
independent reflns.	21133	20802
R(int)	0.1239	0.1220
ind. reflns. ($I > 2\sigma(I)$)	16072	13922
parameters	1092	1070
restraints	180	181
R_1 ($I > 2\sigma(I)$)	0.0826	0.0759
wR_2 (all data)	0.2537	0.2247
GooF (all data)	1.090	1.037
max. peak/hole/e$^-$·Å^{-3}	3.79 /−5.61	2.89 /−4.62
absorption correction type	numerical[17]	numerical[17]
min. /max. transmission	0.078/0.429	0.226/0.551

clusters were detected, such as $[M@Si_{14}]^-$ and $[M@Si_{13}]^-$ (M = Sm, Eu, Gd, Tb, Ho, Yb).[11b] These intermetalloid clusters are discussed as "designer" materials,[11b] since small variations in their composition can significantly manipulate electronic, optical, or magnetic properties. In $[M@Si_{14}]^-$[11a] and $[M@Si_{13}]^-$ tunability of the magnetic moment is assumed to proceed by choosing the type and oxidation state of the incorporated lanthanide ion. Another effect of Ln ion doping has been reported in semiconductors for which changes are caused in the electronic structure, such as significant band gap narrowing.[12]

We have recently extended the class of intermetalloid clusters by the isolation of $[K([2.2.2]crypt)]_4[Eu@Sn_6Bi_8]\cdot 1.1\cdot en$,[13] the first synthetic intermetalloid cluster encapsulating an Ln ion, and the first synthetic example of an isolated, "naked" 14-vertex cage. It represents a fullerane-type mixed main-group metal cluster with one interstitial Eu(II) ion and an $S = 7/2$ ground state.

Herein we report the synthesis and characterization of two novel compounds, $[K([2.2.2]crypt)]_4[Ln@Sn_7Bi_7]_x[Ln@Sn_4Bi_9]_y\cdot 0.7en$ (**1**: Ln = La; $x = 0.70$, $y = 0.30$; **2**: Ln = Ce; $x = 0.39$, $y = 0.61$; *en* = ethylenediamine), that not only differ by another Sn:Bi ratio from the quoted Eu compound but additionally comprise a yet unprecedented cluster type with a 13-atomic Sn/Bi shell embedding an La or Ce ion within their crystal structures. As confirmed by magnetic measurements, the two anions of the Ce compound **2** are paramagnetic intermetalloid clusters. DFT investigations served to analyze the electronic structure of the clusters and to shed light on the nature and effect of the Ln^{3+} interaction with the semimetal cluster shell that allows for the description as doped semimetal cages.

EXPERIMENTAL SECTION

Syntheses. *General.* All manipulations and reactions were performed in an argon or nitrogen atmosphere using standard Schlenk or glovebox techniques. Ethylenediamine (*en*) (Aldrich, 99%) was dried over CaH_2, *p*-xylene (Acros Organics, 99%) was dried over sodium. Both solvents were freshly distilled prior to use. [2.2.2]crypt[14]

dx.doi.org/10.1021/ja209226b | J. Am. Chem.Soc. 2012, 134, 1181−1191

(Merck) was dried in vacuum for 13 h. Tris-(tetramethylcyclopentadienyl)-lanthanum $(C_5Me_4H)_3La$ (Aldrich) and tris-(tetramethylcyclopentadienyl)-cerium $(CpMe_4H)_3Ce$ (Aldrich) were used as received. The precursor $[K([2.2.2]crypt)]_2[Sn_2Bi_2]$·*en* was prepared according to the literature.[15]

Syntheses of [K([2.2.2]crypt)]$_4$[La@Sn$_7$Bi$_7$]$_{0.70}$[La@Sn$_4$Bi$_9$]$_{0.30}$·0.7en (1) and [K([2.2.2]crypt)]$_4$[Ce@Sn$_7$Bi$_7$]$_{0.39}$[Ce@Sn$_4$Bi$_9$]$_{0.61}$·0.7en (2). $[K([2.2.2]crypt)]_2[Sn_2Bi_2]$·*en* (193 mg, 0.125 mmol) was weighed out into a Schlenk tube inside a glovebox and dissolved in *en* (3 mL), resulting in a dark reddish-brown solution. Into another Schlenk tube inside a glovebox, 82 mg (0.163 mmol) of $(C_5Me_4H)_3Ln$ was weighed out and suspended in *p*-xylene (1 mL) to produce a yellow (La) or greenish (Ce) suspension. The latter was added to the precursor solution while stirring vigorously. The reaction mixture was allowed to stir for 3 h. The dark-brown reaction solution was filtered through a standard glass frit and carefully layered by *p*-xylene (4 mL). After 3 days, black rhombus-like plates of $[K([2.2.2]crypt)]_4[La@Sn_7Bi_7]_{0.70}[La@Sn_4Bi_9]_{0.30}$·0.7en (**1**) or $[K([2.2.2]crypt)]_4[Ce@Sn_7Bi_7]_{0.39}[Ce@Sn_4Bi_9]_{0.61}$·0.7en (**2**), respectively, formed at the wall of the Schlenk tube in approximately 30% yield (based on $[K([2.2.2]crypt)]_2[Sn_2Bi_2]$·*en*). No alternative crystallization method, including the employment of further cation sequestering agents, different solvents, or layering techniques, allowed for the separate crystallization of one of the cage-types. It is, however, possible to crystallize a polymorph of both compounds upon layering of the reaction mixture by toluene instead of *p*-xylene. The crystal structures, with approximately twice the unit cell volume (vide infra), are again more complicated and afflicted with more crystallographic problems. One observes the same intrinsic cocrystallization of the 14-atom and the 13-atom cages as in **1** and **2**.

Energy Dispersive X-ray (EDX) Spectroscopy. EDX analyses (Table 1) were performed using an EDX device Voyager 4.0 of Noran Instruments coupled with an electron microscope CamScan CS 4DV. Data acquisition was performed with an acceleration voltage of 20 kV and 100 s accumulation time. For the analyses, multiple single crystals were used, and the data were recorded both various times on one single crystal and various times on other single crystals.

X-ray Diffraction. Single-crystal X-ray diffraction data were collected on a Stoe IPDS2T diffractometer at 100 K with Mo Kα radiation (λ = 0.71073 Å). The structures were solved by direct methods and refined by full matrix least-squares against F^2 using SHELXS-97 and SHELXL-97 software[16] (Table 2). The unit cell dimensions of the polymorphs (crystallized from toluene) are as follows: space group $P2_1/c$; Ln = La: a = 17.604(4) Å, b = 27.763(5) Å, c = 52.105(2) Å, β = 91.04(2)°, V = 25462(11) Å^3; Ln = Ce: a = 17.524(6) Å, b = 27.640(7) Å, c =52.092(2) Å, β = 91.32(3)°, V = 25226(13) Å^3.

Refinement outline for C$_{73.40}$H$_{149.6}$Bi$_{7.6}$K$_4$La$_1$N$_{9.4}$O$_{24}$Sn$_{6.1}$ (1) and C$_{73.40}$H$_{145.50}$Bi$_{8.22}$Ce$_1$K$_4$N$_{9.40}$O$_{24}$Sn$_{5.17}$ (2). For both **1** and **2**, the crystals seem to be isomorphous with the previously investigated Eu-analogue.[13] Therefore, the crystal structure model for the Eu compound was taken as a starting model for the refinements carried out on the La compound **1**. A careful check was carried out in order to exclude the possibility of twinning artifacts. The most striking feature observed at all initial refinement stages is the presence of a difference Fourier maximum of 22.40 e$^-$/Å^3 at the Bi2/Sn2–Bi3/Sn3 bond (1.44 Å from Bi3). Geometrical considerations led to the conclusion that this maximum may arise only from a second 13-vertex cluster, since no model considering rotational disorder with a second 14-vertex cluster could explain this observation. The same feature is observed on starting the crystal structure refinement ab initio or on trying a solution in lower-symmetry space groups.

Initially refined structure parameters (starting from the model applied to the Eu-compound[13]) were fixed, and the highest peak was introduced as Bi atom (in accordance with theoretical studies—see Results and Discussion). The occupancy of this site was refined to a value near 0.35–0.45. Experimental evidence from other methods (see text) indicates that there should be an excess of the 14-vertex cluster with respect to the 13-vertex cluster. Therefore, an occupancy of 0.3 was fixed for this site and 0.7 for the neighboring sites that belong to the 14-vertex cluster as a constraint. Subsequently, a careful refinement of the occupancies of the mixed Sn/Bi sites was undertaken with manual control of their sums and fixing the refined values; due to a large number of parameters, the use of such constraints as SUMP was limited.

Further refinement involved modeling the disorder of the organic part and introducing disordered 1,2-diaminoethane molecules of solvation (for more details see the Supporting Information).

The model obtained for **1** was applied as a starting model for **2** upon substituting Ce for La. It seems to describe the structure well, except for one remaining difference Fourier maximum of about 5 e/Å^3 found at the Bi15/Sn15–Bi5/Sn5 bond (1.10 Å from Bi15), indicating a second position of the 13-vertex cluster. A similar treatment of the structure model as in the case of the additional maximum found at the initial refinement of **1** led to a 0.11 occupancy of the second 13-vertex cluster. Thus, the total 13-vertex cluster content in **2** (13-vertex:14-vertex: 0.61:0.39) was found to be higher in **2** than in **1** (13-vertex:14-vertex: 0.30:0.70).

Electrospray Ionization Mass Spectrometry (ESI-MS) Investigations. ESI-FT-ICR-MS has been performed on a Finnigan LTQ-FT spectrometer by Thermo Fischer Scientific in the negative ion mode: spray voltage 3.90 kV, capillary temperature 300 °C, capillary voltage −11 V, tube lens voltage −108.38 V, with sheath gas. The reaction mixture, after 3 h reaction time, was analyzed in the 1,2-diaminoethane/*p*-xylene solvent mixture. The overview ESI-FT-ICR-MS mass spectra of the reaction mixtures are given in Figures S13 and S26. For the analyses of the products, single crystals of **1** or **2** were dissolved in dimethylformamide at −60 °C (Figure 2), the according overview spectra are given in Figures S39 and S40.

Mössbauer Measurements. A $Ca^{119m}SnO_3$ source was available for the ^{119}Sn Mössbauer spectroscopic investigation. The sample was sealed within a thin-walled glass container at a thickness of about 10 mg Sn/cm^2. A palladium foil of 0.05 mm thickness was used to reduce the tin K X-rays concurrently emitted by this source. The measurement was conducted in the usual transmission geometry at 78 K. The source was kept at room temperature.

Magnetic Measurements. The magnetic susceptibility measurements were obtained with the use of a Quantum Design SQUID magnetometer MPMS-XL housed at the Centre de Recherche Paul Pascal. This magnetometer works between 1.8 and 400 K for dc applied fields ranging from −7 to 7 T. Measurements were performed on polycrystalline samples of 3.60 and 19.55 mg for **1** and **2** respectively, introduced in polyethylene bags (3 cm × 0.5 cm × 0.02 cm) sealed under argon. The magnetic data were corrected for the sample holder (plastic bag for both compounds) and the diamagnetic contribution (only for **2** as **1** is diamagnetic).

Methods of the Quantum Chemical Investigations. The density functional theoretical (DFT) investigations were undertaken by means of the program system TURBOMOLE[18] using the Ridft program[19] with the Becke–Perdew 86 (BP86) functional.[20] Basis sets were of def2-TZVP quality (TZVP = triple-ζ valence plus polarization) for Sn, Bi, La[21] and of ECP28MWB_SEG type for Ce[22a] (with reduced set of g functions). For La (ECP-46),[23] Ce (ECP-28),[22b] Sn (ECP-28)[24] and Bi atoms (ECP-60),[24] effective core potentials have been used for consideration of relativistic corrections and to reduce the computational effort. The high negative charge was compensated for by employment of the COSMO model.[25] Simultaneous optimizations of geometric and electronic structures were performed without symmetry restrictions for $[Ln@Sn_7Bi_7]^{4-}$ and $[Ln@Sn_4Bi_9]^{4-}$ (C_1), also allowing for convergence into local minima at higher symmetry. The calculated interatomic distances are in accordance with the experimentally observed ones within the typical error of the method.

RESULTS AND DISCUSSION

Syntheses. Compounds $[K([2.2.2]crypt)]_4[Ln@Sn_7Bi_7]_x[Ln@Sn_4Bi_9]_y$·0.7en (**1**: Ln = La, x = 0.70, y = 0.30, and **2**: Ln = Ce, x = 0.39, y = 0.61) were obtained by reactions of $[K([2.2.2]crypt)]_2[Sn_2Bi_2]$·*en*[15] with $[(C_5Me_4H)_3Ln]$ (Ln =

dx.doi.org/10.1021/ja209226b | J. Am. Chem.Soc. 2012, 134, 1181–1191

Scheme 1. Syntheses of 1 or 2 (1: Ln = La, x = 0.70, y = 0.30; 2: Ln = Ce, x = 0.39, y = 0.61)

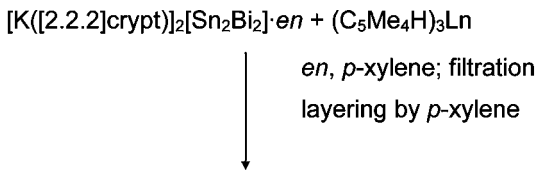

La, Ce) as extremely air- and moisture-sensitive black, rhombus-like crystals (Scheme 1).

Different from a similar reaction with $[(C_5Me_4H)_3Eu]$, the reactions presented herein result in the formation and cocrystallization of two different enneahedra, $[Ln@Sn_7Bi_7]^{4-}$ and $[Ln@Sn_4Bi_9]^{4-}$. Additionally, no redox process was observed during the reaction, whereas for the reported Eu complex, a reduction took place from Eu(III) to Eu(II). The formal +III oxidation state of both La and Ce ions was confirmed by magnetic measurements (vide infra), that indicate a diamagnetic La compound and a paramagnetic Ce compound.

Composition and Structures. In addition to $[Eu(II)@Sn_6Bi_8]^{4-}$, the $[Ln@Sn_7Bi_7]^{4-}$ anions in **1** and **2** (Figure 1) represent the second example of an isolated, ligand-free 14-vertex enneahedron, consisting of six pentagons and three square faces; however, in accordance with the different charge of the encapsulated Ln cation, it possesses a different Sn/Bi composition than the previously reported cluster. The second species present in the crystal structure, $[Ln@Sn_4Bi_9]^{4-}$, represents another type of enneahedron, with an unprecedented combination of five square faces and four pentagons. Four of the square faces are strongly distorted (angles for **1**: 74.5(1)−98.9(1)°, for **2**: 69.6(3)−104.6(1)°) and meet at one main group atom (Bi1), which is the only four-bonded position within the anionic cages of the title compounds. Selected distances and angles of the cluster anions in compounds **1** and **2** are summarized in Tables S1 and S2 in the Supporting Information.

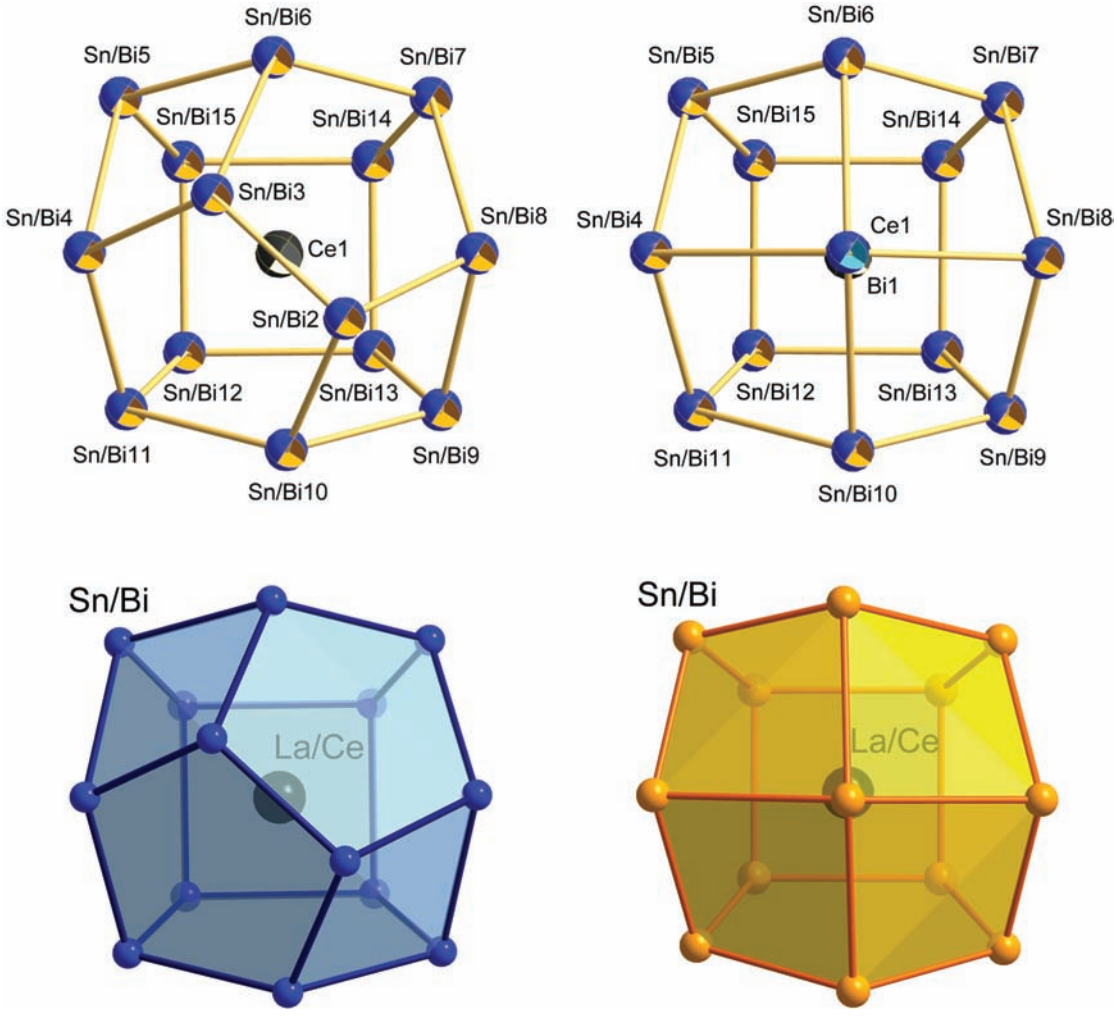

Figure 1. Molecular structures of $[Ce@Sn_7Bi_7]^{4-}$ (left) and $[Ce@Sn_4Bi_9]^{4-}$ (right) as examples for the molecular cluster anions in **1** and **2** in ball-stick representation (top, orange/blue spheres denote Sn/Bi mixed sites) and polyhedral representation (bottom). Disorder is not shown for clarity (for more details and displacement ellipsoid plots see Supporting Information). Averaged bond lengths in **1** /Å: $[La@Sn_7Bi_7]^{4-}$: Sn/Bi−Sn/Bi 2.870(3)−3.014(3); La−Sn/Bi 3.424(2)−3.585(3); $[La@Sn_4Bi_9]^{4-}$: Sn/Bi−Sn/Bi 2.925(2)−3.009(2); La−Sn/Bi 3.424(2)−3.557(2); Bi1−Sn/Bi(4,6,8,10) 3.514(5)−3.604(5); La−Bi1 3.107(4). Averaged bond lengths in **2** /Å: $[Ce@Sn_7Bi_7]^{4-}$: Sn/Bi−Sn/Bi 2.849(4)−3.015(2); Ce−Sn/Bi 3.402(2)−3.543(3); $[Ce@Sn_4Bi_9]^{4-}$: Sn/Bi−Sn/Bi 2.897(2)−3.015(2); Ce−Sn/Bi 3.402(2)−3.538(2); Bi1−Sn/Bi(4,6,8,10) 3.481(3)−3.504(3); Ce−Bi1 3.04(2)−3.057(3).

dx.doi.org/10.1021/ja209226b | J. Am. Chem.Soc. 2012, 134, 1181−1191

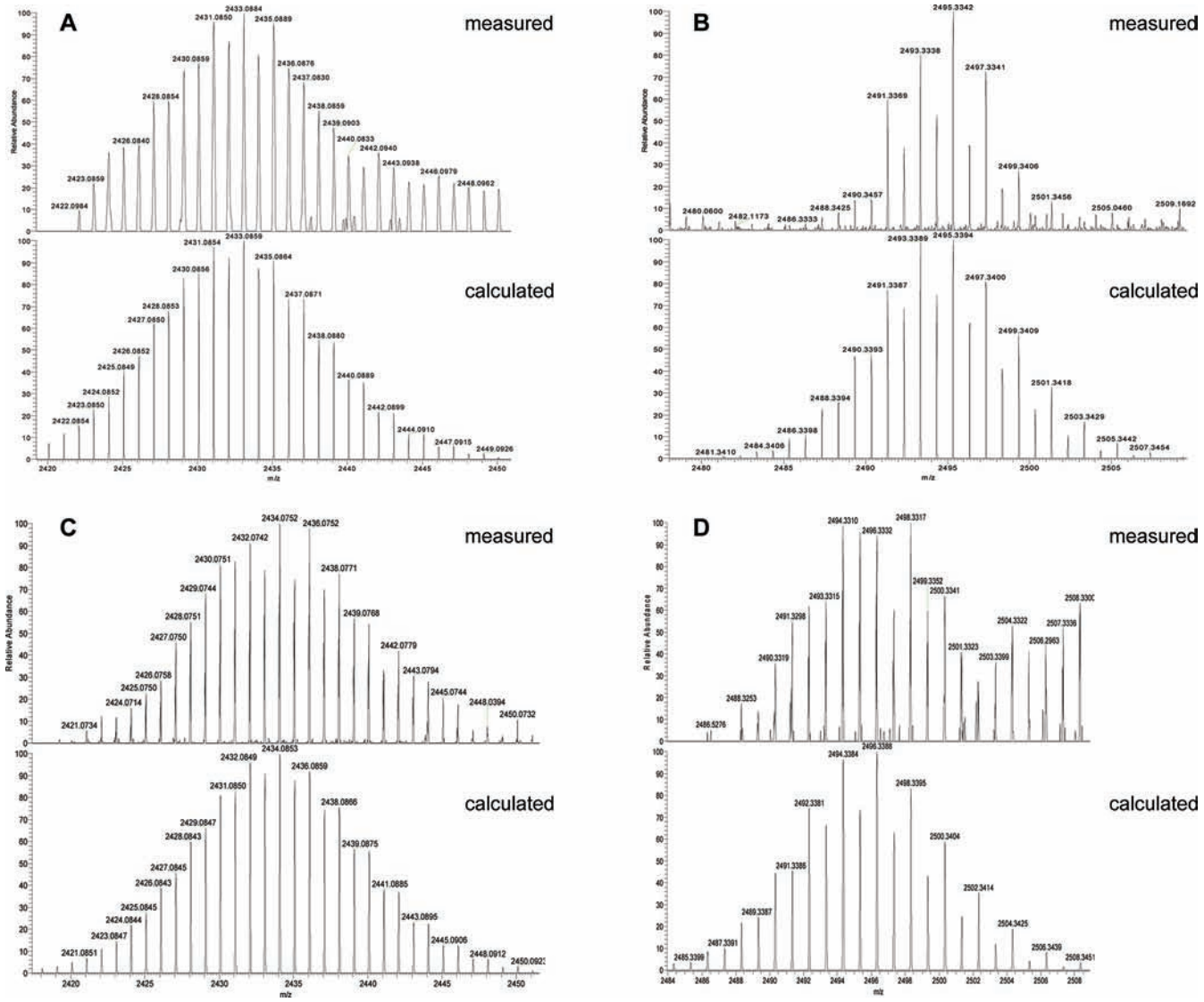

Figure 2. ESI-MS spectra of the anions in **1** and **2**, $[La@Sn_7Bi_7]^-$ (A), $[La@Sn_4Bi_9]^-$ (B), $[Ce@Sn_7Bi_7]^-$ (C), $[Ce@Sn_4Bi_9]^-$ (D).

The first hint on the existence of the new 13-vertex species was provided by the X-ray diffraction studies (see Experimental Section and Supporting Information). The studies carried out for multiple crystals combined with the use of other techniques confirmed the presence of the 13-vertex anion and excluded the possibility of a rotational disorder of another 14-vertex to explain the observations during the structure refinement. The studies also agree in the finding of different relative amounts of the two clusters in the crystals of **1** and **2**. Whereas the 14-vertex cluster anion (70%) occurs in higher amount with respect to the 13-vertex cluster (30%) for Ln = La, the situation is different for Ln = Ce. Here, the 14-atom enneahedron, which is superimposed by two 13-vertex enneahedra, represents the minority (39%), whereas the latter represents the majority (61%). The reason for this is not clear yet, but the observation is completely reproducible on different crystals, thus most likely due to the differing ionic radii of La^{3+} or Ce^{3+}, respectively.

In addition to the described mixture of the two anionic species in the crystal structure, one also faces disorder of the Sn and Bi atomic sites. Heavy statistical and/or rotational disorder of the two different main group elements is known from our previous investigations on ternary intermetalloid clusters,[26] and also from the binary starting material[15] – more pronounced with an increasingly spherical shape of the binary cage. Due to the cocrystallization and superimposition of two slightly different enneahedra, the situation is even more complicated here, which required a sophisticated combination of analytical techniques. The Sn:Bi ratio of the two different enneahedra were determined by electrospray ionization Fourier transform ion cyclotron resonance mass spectrometry (ESI-FT-ICR-MS) of single crystals of **1** and **2** dissolved in dimethylformamide (Figure 2 and Figures S39, S40 in Supporting Information). This study revealed $[Ln@Sn_7Bi_7]^-$ and $[Ln@Sn_4Bi_9]^-$ to be the dominating species, beside a minority of further cluster anions like $[Ln@Sn_6Bi_8]^-$ and $[Ln@Sn_3Bi_{10}]^-$. However, the 4– charge of the cluster anions, which was determined by the number of counterions in the crystal structure, helps to exclude the presence of the latter two species in the solid state: possessing an odd total electron number, both $[La@Sn_6Bi_8]^{4-}$ and $[La@Sn_3Bi_{10}]^{4-}$ would result in the occurrence of notable amounts of paramagnetic impurities, which were not observed in the magnetic measurement of compound **1**. In the case of compound **2**, the two compositions would accordingly result in diamagnetic impurities falsifying the applied molecular weight,

dx.doi.org/10.1021/ja209226b | J. Am. Chem.Soc. 2012, 134, 1181–1191

also in disagreement with the magnetic measurements. We therefore assume, that the additionally observed cluster anions with an Sn:Bi ratio of 6:8 or 3:10 were formed upon solution of the title compounds in dimethylformamide or even during the ESI-FT-ICR-MS experiment itself, by fragmentation/rearrangement of the cluster anions in **1** or **2**; in solution, the anions may adopt any charge that fits to the composition, which allows for a larger number of different species to exist, whereas in the crystal structure, the anions are restricted to a composition that accords to the 4− charge. According to our findings, this seems to be stable only with the 7:7 and 4:9 atomic Sn:Bi ratio.

^{119}Sn Mössbauer Spectroscopy, Magnetic Properties and Electronic Structures. Figure 3 shows the ^{119}Sn Mössbauer spectrum of compound **1** at 77 K. Similar to that of the $[Sn_2Bi_2]^{2-}$ cluster,[15,27] the spectrum can be fitted with

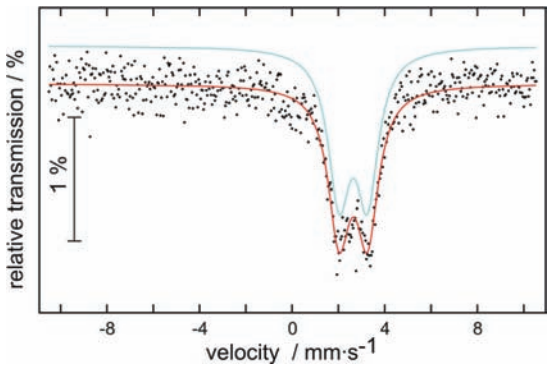

Figure 3. Experimental and simulated ^{119}Sn Mössbauer spectrum of **1** at 77 K.

one quadrupole split Sn site with the fitting parameters listed in Table 3. The spectrum shows a single signal at an isomer shift of 2.65 mm/s subjected to electric quadrupole splitting of 1.22 mm/s, reflecting the noncubic-site symmetry of the tin atoms.

Table 3. Fitting Parameters of a ^{119}Sn Mössbauer Spectroscopic Measurement of 1[a]

T/K	δ/mm·s^{-1}	Γ/mm·s^{-1}	ΔE_Q/mm·s^{-1}
77	2.65(1)	1.14(4)	1.22(2)

[a]Numbers in parentheses represent the statistical errors in the last digit. (δ), isomer shift; (Γ), experimental line width, (ΔE_Q), electric quadrupole splitting parameter.

Since the structure contains a number of crystallographically independent Sn atoms, the ^{119}Sn spectrum is a superposition of almost equal subspectra which cannot be resolved. All possible isomers of the clusters $[Ln@Sn_7Bi_7]^{4-}$ and $[Ln@Sn_4Bi_9]^{4-}$ in compound **1** (vide infra) are quite similar concerning the electronic situation at the Sn nuclei from the perspective of Mössbauer spectroscopy. For this reason, a differentiation between and correlation to individual isomers of the clusters is not possible. As in $[Sn_2Bi_2]^{2-}$, the isomer shift is slightly increased with respect to α-Sn (2.02 mm/s) and β-Sn (2.54 mm/s)[28] with neutral Sn atoms, underlining the *stannide* nature of the Sn atoms in the clusters.

Magnetic susceptibility measurements have been performed to confirm the formal oxidation states of the lanthanide ions and thus the charge of the Sn/Bi shell. These measurements on **1** reveal its diamagnetic nature in accordance with the even electron number of $[La@Sn_7Bi_7]^{4-}$ and $[La@Sn_4Bi_9]^{4-}$ and thus a +III oxidation state of the La ions. Its diamagnetic susceptibility is −0.0069 cm^3/mol and the ultrapurity of the sample should be highlighted as only 0.45% of S = 1/2 magnetic impurity has been detected (Figure S12). On the other hand, **2** displays a paramagnetic behavior as expected for Ce(III) cations (Figure 4).

At room temperature, the χT product is equal to 0.83 cm^3 K mol^{-1} which is in very good agreement with the presence of one

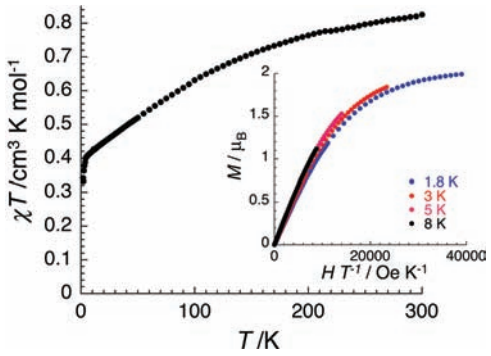

Figure 4. Temperature dependence of the χT product for **2** at 1000 Oe (with χ being the molar magnetic susceptibility defined as M/H per one Ce center). Insert: Magnetization versus H/T plot between 1.8 and 8 K for **2**.

Ce(III) metal ion (C_{Ce} = 0.8 cm^3 K mol^{-1}).[29] When the temperature is lowered, the χT product at 1000 Oe decreases continuously down to 0.32 cm^3 K mol^{-1} at 1.8 K. This type of thermal dependence of the magnetic susceptibility is expected for Ce(III) metal ions that possess strong ligand field effects that splits its J = 5/2 ground-state multiplet into $2J$ + 1 sublevels. The decrease of the temperature leads to a progressive thermal depopulation of the excited (more magnetic) sublevels and thus to a decrease of the χT product. Below 8 K, the field dependence of the magnetization (inset of Figure 4) is not completely saturated under 7 T even at 1.8 K and reaches 2 μ_B in very good agreement with the magnetization expected at saturation (M_{sat} = Jg_J = 2.14 μ_B) for Ce(III) ions. All these measurements confirm without ambiguity the presence of Ce(III) in **2**.

Unlike our previous findings for $[Eu@Sn_6Bi_8]^{4-}$, the lanthanide ions were neither reduced nor oxidized during the reactions but retained their formal +III oxidation state. This observation is in accordance with compounds like $Eu@C_{82}$ and $La@C_{82}$;[30] the latter possess formal oxidation states Eu(II) and La(III), as expected. The presence of Ln(III) ions comes along with diamagnetic main group atom shells in the 14-vertex enneahedra $[Ln^{3+}@(Sn_7Bi_7)^{7-}]^{4-}$ (Ln = La, Ce), representing electron-precise anions in agreement with the Zintl−Klemm−Busmann pseudoelement concept.[31]

The situation is significantly different for the 13-atom enneahedra. The assignment of charges according to $[Ln^{3+}@(Sn_4Bi_9)^{7-}]^{4-}$ (Ln = La, Ce) does not correlate with the simple assignment of three-bonded Sn^- or Bi^0 and four-bonded Sn^0 or Bi^+ atoms. Considering a Bi^+ atom to be located on the four-bonded position, the pseudoelement treatment would result in a $(Sn_4Bi_9)^{3-}$ cluster shell; with Sn^0 at this position, the binary shell would accord to $(Sn_4Bi_9)^{4-}$—both in disagreement with the total charge. However, quantum chemical investigation helped to clarify both the assignment of atoms and the charge distribution (vide infra).

dx.doi.org/10.1021/ja209226b | J. Am. Chem.Soc. 2012, 134, 1181−1191

The formation of the 14-atom enneahedron $[Ln@Sn_7Bi_7]^{4-}$ might involve two nortricyclane-type seven-atom Zintl anionic precursors, $[Sn_3Bi_4]^{6-}$ and $[Sn_4Bi_3]^{7-}$, that seem to form by fragmentation/aggregation processes upon addition of the Ln precursor, as discussed for $[Eu@Sn_6Bi_8]^{4-}$ based on ESI-MS investigations of the reaction mixture.[13] The ESI mass spectrum of the reaction mixture that leads to the formation of **1** (Ln = La) indeed shows signals of both fragments that might combine in the presence of the La^{3+} ion. For the 13-vertex enneahedra, an according combination of rearranged precursor species is also plausible. This would involve at least in part fragments which do not represent known Zintl-type anions, such as the combination of (i) a six-atom and a seven-atom fragment or (ii) an eight-atom and a five-atom fragment. As for all ESI-MS studies performed on our reaction mixtures so far, those leading to the formation of **1** and **2** also show predominance of a nine-atom species $[Sn_6Bi_3]$ after three hours reaction time, which, however, cannot play a direct role in the generation of the Sn-poorer 13-vertex clusters. Further species of significant intensity with lower numbers of Sn atoms are $[Sn_2Bi_3]$ and $[Sn_3Bi_5]$ (Ln = La) or $[Sn_2Bi_3]$ and $[Sn_2Bi_5]$ (Ln = Ce)—again not matching with the resulting composition of the second cluster anion. A weaker peak can be assigned to the species $[Sn_2Bi_6]$ in the mixture that yields compound **2**; a Ce^{3+} ion located between $[Sn_2Bi_6]$ and $[Sn_2Bi_3]$ fragments might lead to the closure of the two hemispheres to give the 13-vertex cluster observed in **2**. Since the fragments of relevance are only observed in small amounts beside the predominant $[Sn_6Bi_3]$ species, it is plausible that fragments that might aggregate to a 14-atom cluster shell are only detected in the reaction mixture of compound **1**—with a majority of the 14-vertex cluster anion—whereas fragments that might represent precursors to the 13-atom cluster shell are only observed in the reaction mixture that yields compound **2**—with a majority of the 13-vertex cluster anions.

Both polyhedra with 14 or 13 vertices are rare. Molecular polyhedra with more than 12 atoms comprise the Frank Kasper-type[32] carborane [*closo*-1,2-$(CH_2)_3$-1,2-$C_2B_{12}H_{14}$][33] or the wheel-shaped cluster $[Al_{14}\{N(SiMe_3)_2\}_6I_6Li(OEt_2)_2]^-$.[34] Molecular cages with vertex number 13 are even more unusual. There exist some metallacarborane examples, such as 4,1,6-*closo*-$SnC_2B_{10}H_{12}$ or 1,6-Me_2-4,1,6-*closo*-$SnC_2B_{10}H_{10}$.[35] Carborane clusters with 13 vertices have been unknown until the isolation of 1,2-μ-$\{C_6H_4(CH_2)_2\}$-3-Ph-1,2-$C_2B_{11}H_{10}$ in 2003.[36] The latter adopts the geometry of a henicosahedron. None of these examples represent "naked" clusters without organic ligands and none of them comprise interstitial atoms. Coordination numbers larger than 12 are also very rare and only known in extended solids, such as the Friauf-Laves phases,[37] or within liquid metals according to simulations.[38]

Endohedral clusters $[M_x@E_n]$ ($n \geq 9$) might be viewed as coordination compounds of the interstitial metal atom with a spherical ligand shell, if there are significant covalent M–E-bonding interactions. However, this has not been investigated for all known examples. For systems with a large number of surface atoms, such as endohedral fullerenes like $La@C_{60}$,[39] there are definitely no covalent bonds, but with smaller clusters, one reaches the border between encapsulated ions and M–E-dominated systems. Clusters of the type $[M(ZnR)_n(ZnR')_{12-n}]$ (M = Mo, Ru, Rh, Ni, Pd, Pt; n = 8–12; R = Me, Et, η^5-$C_5(CH_3)_5$ = Cp*) for instance, were rather discussed as coordination compounds with an n-coordinated M atom,[40] whereas in $[M@Pb_{10}]^{2-}$ (M = Ni),[41] $[M@Pb_{12}]^{2-}$ (M = Ni, Pd, Pt),[7] or $[M@Ge_{10}]^{3-}$ (M = Fe, Co)[42] covalent bonds were mainly detected between the cluster surface atoms which embed a rather isolated M atom. Thus, a sophisticated study of the electronic situation is needed in every single case to explain the nature and resulting properties of such cluster anions.

The magnetic studies gave a first hint toward rather ionic interactions of the interstitial Ln atoms with the binary cages in the cluster anions of the title compounds. In order to verify this assumption, DFT investigations of the anions in **1** and **2** were undertaken. Since the crystallographic result was afflicted with disorder, it was first necessary to explore the most probable $[Sn_7Bi_7]$ or $[Sn_4Bi_9]$ atomic distribution within the 14-atom or the 13-atom cluster shells.

This point was investigated for $[La@Sn_7Bi_7]^{4-}$ and $[Ce@Sn_7Bi_7]^{4-}$ by simultaneous optimizations of the geometric and electronic structures of all 329 isomers with different $[Sn_7Bi_7]$ atomic distributions (Supporting Information). The study indicated the aggregation pattern of the Sn atoms and its arrangement on the cluster surface to be the most relevant parameter. For both Ln = La and Ce as interstitial atom, isomers with two Sn–Sn dumbbells and three isolated Sn atoms distributed over the 14-atom shell turned out to be the most stable ones—leading to a shortlist of nine isomers for each kind of lanthanide ion that exhibit the most likely positions of Sn and Bi atoms on the $[Ln@Sn_7Bi_7]^{4-}$ cluster surfaces (Figures 5 and 6). An explanation for this might be the balance between the tendency to maximize the number of Bi–Sn or Bi–Bi bonds—being more stable than Sn–Sn bonds

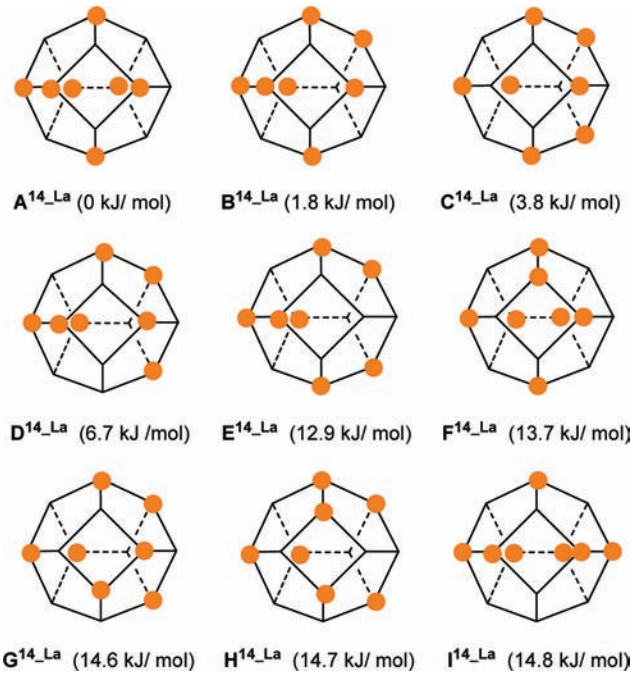

Figure 5. Nine most stable isomers of $[La@Sn_7Bi_7]^{4-}$, according to DFT investigations. Relative energies ΔE are given with respect to the most stable isomer $\mathbf{A}^{14\_La}$. The clusters are drawn schematically without interstitial La atom; orange spheres represent Sn atoms.

(210.0 or 200.4 versus 187.1 kJ·mol^{-1})[43]—and geometric requirements that seem to prefer the presence of some short Sn–Sn contacts. Despite the sequence of relative stabilities being slightly different for $[La@Sn_7Bi_7]^{4-}$ or $[Ce@Sn_7Bi_7]^{4-}$, respectively, four of the isomers show energy differences within the error of the quantum chemical method for both systems. At

dx.doi.org/10.1021/ja209226b | J. Am. Chem.Soc. 2012, 134, 1181–1191

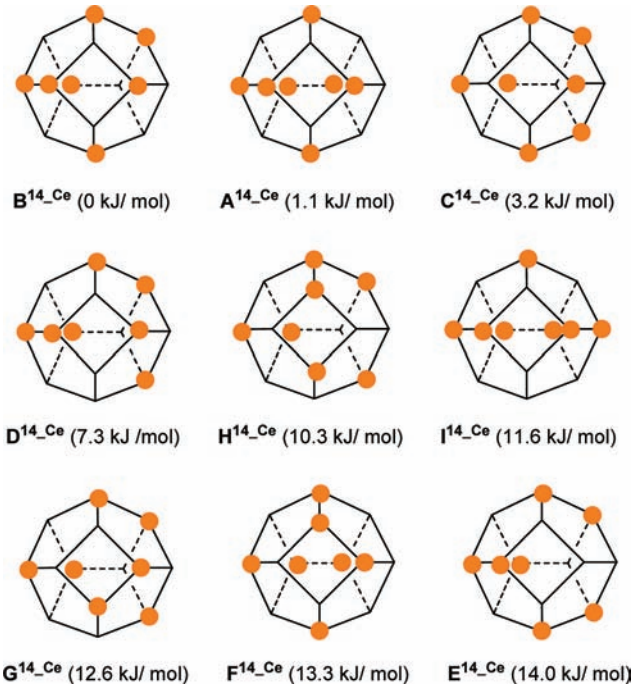

Figure 6. Nine most stable isomers of $[Ce@Sn_7Bi_7]^{4-}$, according to DFT investigations. Relative energies ΔE are given with respect to the most stable isomer $\mathbf{B}^{14\_Ce}$. The clusters are drawn schematically without interstitial Ce atom; orange spheres represent Sn atoms.

this point, it is still not clear whether the anions in **1** and **2** might accord to the most stable isomers (A^{14_La} / B^{14_Ce}), or to a statistical mixture of these most likely isomers.

For the 13-atom enneahedra $[Ln@Sn_4Bi_9]^{4-}$, all 111 isomers for Ln = La and Ln = Ce, respectively, have been calculated by DFT methods (Supporting Information). Due to the lower symmetry and the additional four-bonded site, two further crucial parameters regarding the position of Sn atoms on the 13-atom shell emerged for this composition: First, a preference of the placement of Sn atoms at positions most distant from the four-bonded Bi site and second, preferred placement of Sn atoms on nonequivalent positions. Vice versa, a Bi atom is clearly favored on the four-bonded position (Bi1); due to considerable sterical strain for the smaller tin atom at the four-bonded position, these isomers are all by at least 71 $kJ \cdot mol^{-1}$ less stable. As a result, only three isomers—identical for both $[La@Sn_4Bi_9]^{4-}$ and $[Ce@Sn_4Bi_9]^{4-}$—show relative energies within the error of the employed quantum chemical method (Figure 7). The two most stable isomers differ only in one Sn position, resulting in a relative energy for the second isomer of +8 $kJ \cdot mol^{-1}$ (Ln = La) or +12 $kJ \cdot mol^{-1}$ (Ln = Ce) with regard to the most stable isomers $\mathbf{A}^{13\_Ln}$. Thus, the atomic distribution of Sn and Bi is determined more precisely in the 13-atom enneahedral cages of $[Ln@Sn_4Bi_9]^{4-}$ than in $[Ln@Sn_7Bi_7]^{4-}$ and $[Eu@Sn_6Bi_8]^{4-}$.

As mentioned above, the 13-vertex clusters do not allow for an assignment of formal charges regarding the simple pseudoelement concept. Disagreement with this concept is known for many Zintl anions, also including well-known homoatomic ones like the $[E^{14}_9]^{3-/4-}$ family.[44] However, whereas the disagreement requires the application of Wade–Mingos rules[45] in the case of $[Sn_9]^{4-}$, for the title compounds, other kinds of "electron-precise" 13-vertex cluster anions that do accord to the Zintl–Klemm–Busmann concept[31] result

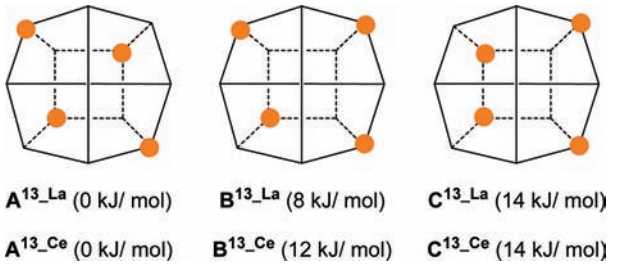

Figure 7. Three most stable isomers of $[Ln@Sn_4Bi_9]^{4-}$, according to DFT investigations. Relative energies ΔE (top: Ln = La; bottom: Ln = Ce) are given with respect to the most stable isomer $\mathbf{A}^{13\_Ln}$. The clusters are drawn schematically without interstitial Ln atom; orange spheres represent Sn atoms.

from two different ways of charge assignment: (a) upon a formal split-up into an $(Sn_4Bi_8)^{4-}$ fragment and two atomic ions, Ln^{3+} and Bi^{3-} (Bi1), with only weak attachment of the latter to the main group fragment, but stronger interaction with the interstitial cation, or (b) by considering the cluster shell as $(Sn_4Bi_9)^{7-}$, however with highly polarized bonds toward Bi1, resulting in a four-bonded Bi^{+} and four rather two-bonded Bi^{-} neighbors. Quantum chemical investigations served to rationalize the second model as follows.

The bond situation was explored by inspection of localized molecular orbitals (LMOs), generated with the technique suggested by Boys.[46] We note in advance that other localization procedures, like that of Pipek and Mezey,[47] yield similar LMOs; the results are qualitatively the same. In the first step, the localization procedure was carried out for the valence orbitals of $[Ln@Sn_7Bi_7]^{4-}$ (this compound has [7·4 (Sn) + 7·5 (Bi) + 1·3 (Ln) + 1·4 (charge)] electrons = 70 valence electrons, i.e. 35 valence orbitals). It leads to one free electron pair at each of the 14 Bi/Sn atoms (more than 95% of the electron density is assigned to the corresponding atom by Mulliken population analysis[48] of the respective LMO, the missing ~5% here and in the following usually are mainly found at the next neighbors) and 21 two-electron-two-center (2e2c) bonds along the 21 edges of the enneahedron. The Sn–Bi bonds show somewhat polarized character, typically 35% contribution from Sn, 60% from Bi, which is similar as e.g. in ClF (40% from Cl, 60% from F); the homoatomic bonds are almost nonpolar (contributions between 45% and 50% from each bond partner); contribution of the central atom to these LMOs is very small (below 5%). Typical LMOs of $[La@Sn_7Bi_7]^{4-}$ are shown in Figure 8 (top).

We note in passing, that contribution from the interstitial Ln atom is slightly larger for Ln = Ce (approximately 6%) which may be rationalized by the somewhat lower energy of the electron-accepting s and d orbitals at Ce^{3+} compared to La^{3+}; calculation within the COSMO model yields −1.49 (−3.65) eV for the 6s (5d) orbitals of La^{3+} and −1.83 (−3.85) eV in case of Ce^{3+}.

The results thus confirm that the description of the system as "Ln^{3+} plus $[Sn_7Bi_7]^{7-}$" is reasonable and that the pseudoelement concept[31] is applicable in this case. Consequently, results for $[Bi_{14}]^{\pm 0}$, which are obtained by replacement of Sn^{-} with Bi and omitting La^{3+}, are qualitatively identical (Figure 8, bottom); the main difference is that here all 2e2c bonds are nonpolar.

We may use these facts to investigate the more complicated bonding situation in $[Ln@Sn_4Bi_9]^{4-}$ in the following way. We first discuss the LMOs of the $[Bi_{13}]^{3-}$ cage obtained from $[Ln@Sn_4Bi_9]^{4-}$ by replacement of Sn^{-} with Bi and omitting Ln^{3+}, and

dx.doi.org/10.1021/ja209226b | J. Am. Chem.Soc. 2012, 134, 1181–1191

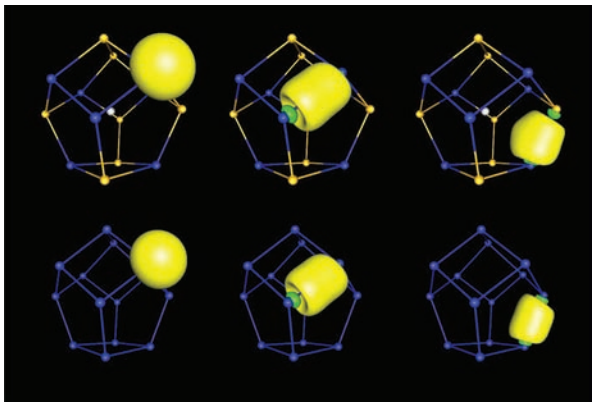

Figure 8. Typical localized molecular orbitals (LMOs) of $[La@Sn_7Bi_7]^{4-}$ (most stable isomer, top) and the hypothetical $[Bi_{14}]^{\pm0}$ cage (bottom): one of the 14 free electron pairs at the 14 main group atoms (left-hand side) and two of the 21 LMOs on the 21 edges in $[La@Sn_7Bi_7]^{4-}$ or $[Bi_{14}]^{\pm0}$, respectively. A nonpolar Bi−Bi bond (center) and a Bi−Sn bond which is slightly polarized in $[La@Sn_7Bi_7]^{4-}$, while nonpolarized in $[Bi_{14}]^{\pm0}$ (right-hand side). Amplitudes are drawn to 0.07 a.u. Color code of vertices and adjacent bond parts: Bi: blue, Sn: orange, La: gray.

then consider the (small) changes resulting from adding Ln^{3+} and re-exchanging Bi with Sn^-. The 34 valence MOs of $[Bi_{13}]^{3-}$ yield the following 34 LMOs (Figure 9, top): one free electron pair at each of the atoms Bi2−Bi13 (left column in Figure 9; numbers according to Figure 1) and 16 covalent bonds

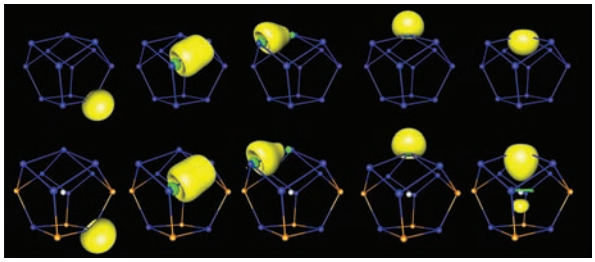

Figure 9. Typical localized molecular orbitals (LMOs) of a hypothetical $[Bi_{13}]^{3-}$ cage (top) and of $[La@Sn_4Bi_9]^{4-}$ (most stable isomer, bottom): a free electron pair (left-hand side), a nonpolar Bi−Bi bond (second from left), one of the strongly polar bonds involving the top Bi1 atom (center), and the two free electron pairs at Bi1 (second from right and right-hand side). One of the latter is delocalized toward the d_{z^2}-orbital of the interstitial La atom in the case of $[La@Sn_4Bi_9]^{4-}$. See also Figure 8.

between these atoms (second column from left); so far, the situation is the same as for $[Bi_{14}]^{\pm0}$. The remaining six LMOs involve the top atom Bi1. Among them, one finds two free electron pairs at Bi1 (first and second column from right) and four bonds from Bi1 to Bi4, Bi6, Bi8, and Bi10 (central column), which are strongly polarized toward these atoms; a Mulliken population analysis yields approximately 20% electrons for Bi1 and 75% electrons for the respective bond partner. For comparison we note that for the—strongly polarized—bond in HF one obtains 30% (70%) at the H (F) atom, the respective values for (ionic) AgF are 18% and 82%. If one is interested in assigning formal oxidation states, the assignment which is best justified by the calculations is Bi^{1-} for "two-bonded" Bi4, Bi6, Bi8, Bi10, and Bi^{1+} for four-bonded Bi1—both in agreement with the pseudoelement concept. Resubstitution of Bi with Sn^- does not qualitatively change this picture but only leads to polarization of the Sn−Bi bonds (as for $[Sn_7Bi_7]^{7-}$, see above). The interaction of the Ln atom with the surrounding cage in $[Ln@Sn_4Bi_9]^{4-}$ mainly is similar to that in $[Ln@Sn_7Bi_7]^{4-}$, i.e. it represents an Ln^{3+} ion with a surrounding $[Sn_4Bi_9]^{7-}$ shell.

Closer inspection of the LMOs of $[Ln@Sn_4Bi_9]^{4-}$ (Figure 9, bottom), shows a delocalization of the second free electron pair of Bi1 to the empty d_{z^2}-orbital of Ln (75% from Bi1, 16% from Ln for Ln = La, first column from right in Figure 9), and additionally a delocalization of the electron-rich part of each of the four polarized bonds Bi1−Bi4, Bi1−Bi6, Bi1−Bi8, Bi1−Bi10 toward the central Ln atom (Figure 9, center), leading to a contribution of approximately 4% from Ln = La, whereas the contributions from Bi4,6,8,10 are somewhat reduced. For Ln = Ce this delocalization again is slightly larger (contribution to the LMO involving Ce and Bi1: 17%, contribution to the polarized Bi−Bi bonds: 6%), similar to those observed for the 14-vertex clusters.

Figure 10 shows the density of states (DOS) calculated from the energies of the molecular orbitals (MOs) and their Mulliken charge distributions as well as the MO diagrams for the two endohedral Ln clusters $[Ln@Sn_7Bi_7]^{4-}$ and $[Ln@Sn_4Bi_9]^{4-}$. The DOS curves regarding all atoms show a similar signature, but the atom-type-based graphs differ in detail, owing to the different Sn:Bi ratios and geometries.

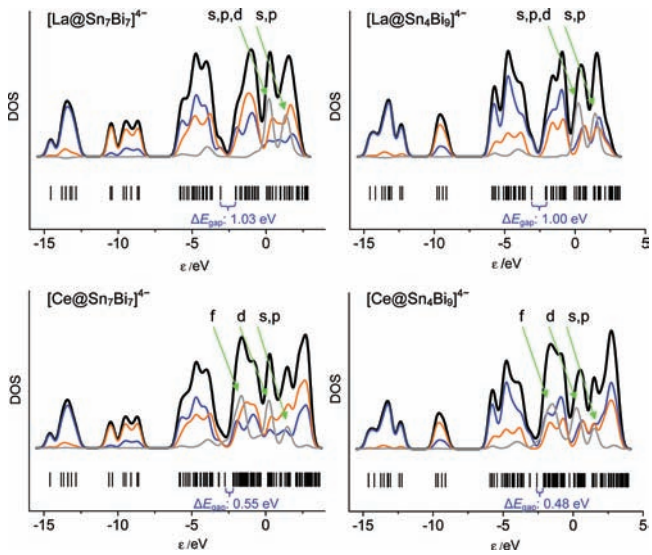

Figure 10. Calculated density of states (DOS) for $[Ln@Sn_7Bi_7]^{4-}$ (left) and $[Ln@Sn_4Bi_9]^{4-}$ (right) for all atoms (black lines), Bi atoms (blue lines), Sn atoms (orange lines), and Ln atoms (gray lines). Dominant atomic orbital types of the contributions to the Ln DOS are indicated.

When comparing the DOS graphs and MO diagrams for Ln = La or Ce, respectively, the most obvious difference is found around the HOMO−LUMO energy gap ΔE_{gap}. The effect of the incorporation of Ce^{3+} instead of La^{3+} comprises the addition of one donor MO energy level (approximately in the middle of the energy gap for Ln = La) that hosts the Ce^{3+} unpaired electron, and the presence of a low-energy acceptor level by the unoccupied f-AOs of the Ce atom whereas La atomic orbitals do not significantly contribute to the LUMO level. As a consequence, ΔE_{gap} amounts to 1.03 or 0.99 eV for the clusters with interstitial La ion, whereas for the interstitial

dx.doi.org/10.1021/ja209226b | J. Am. Chem.Soc. 2012, 134, 1181−1191

Ce atom ΔE_{gap} is only about half that value, 0.55 or 0.49 eV. Thus, the Ce-containing clusters behave like stoichiometrically doped semimetal cages (1:14/1:13 atoms) with an additional donor orbital level to narrow the energy gap. This is in agreement with observations that Ce^{3+} causes band gap narrowing in highly doped semiconductors, such as a red shift of 1 eV in TiO_2—thereby extending the photoactivity to visible light[12]—whereas doping with La^{3+} does not affect the band gap; however, the latter enhances the light absorption of respective suspensions in water.[49]

We summarize that lanthanide ions incorporated in main-group metal cages enable flexibility in structural features and physical properties, due to different electronic configurations and different radii of the incorporated interstitial lanthanide ion. Non-deltahedral 14-vertex or 13-vertex clusters were obtained by embedding interstitial La(III) or Ce(III). Comparison with a related anion incorporating Eu(II) shows that the lanthanide ions cause adjustable variations in the magnetic and electronic properties subject to the varying number of unpaired electrons. Hence, diamagnetic (La) or paramagnetic ground states (Ce, Eu) were stabilized. The clusters presented here are best described as Ln^{3+}-doped (semi) metal cages with polarized Sn−Bi bonds in the cage. In particular, the four-bonded atom, Bi1, of the unique, less isotropic anion $[Ln@Sn_4Bi_9]^{4-}$, shows polarized bonds to its bond partners (also Bi atoms), and a delocalization of one of its lone pairs toward the empty d_{z^2}-orbital orbital of Ln^{3+}, leading to an alternative pseudo-element view of this system.

■ ASSOCIATED CONTENT

Supporting Information

Displacement ellipsoid plots of the anions in **1** and **2** and crystal structure diagrams; additional information on the quantum chemical investigations; on the magnetic measurements of **1**; and details of the ESI-MS investigations of the reaction mixtures affording **1** and **2**. This material is available free of charge via the Internet at http://pubs.acs.org.

■ AUTHOR INFORMATION

Corresponding Author

dehnen@chemie.uni-marburg.de

■ ACKNOWLEDGMENTS

We thank the German Science Foundation (DFG), the Fund of the Association of the Chemical Industry (FCI, Chemiefonds-Stipendium for F.L.), the University of Bordeaux, the Region Aquitaine, the GIS Advanced Materials in Aquitaine (COMET Project), and the CNRS for financial support.

■ REFERENCES

(1) Shinohara, H. *Rep. Prog. Phys.* **2000**, *63*, 843−892.
(2) (a) Stephens, P. W.; Mihaly, L.; Lee, P. L.; Whetten, R. L.; Huang, S.-M.; Kaner, R.; Deiderich, F.; Holczer, K. *Nature* **1991**, *351*, 632−634. (b) Haddon, R. C. *Acc. Chem. Res.* **1992**, *25*, 127−133. (c) Chen, G.; Goddard III, W. A. *Proc. Natl. Acad. Sci. U.S.A.* **1993**, *90*, 1350−1353.
(3) Fässler, T. F.; Hoffmann, S. D. *Angew. Chem.* **2004**, *116*, 6400−6406; *Angew. Chem., Int. Ed.* **2004**, *43*, 6242−6247.
(4) Korber, N. *Angew. Chem.* **2009**, *121*, 3262−3264; *Angew. Chem., Int. Ed.* **2009**, *48*, 3216−3217.
(5) (a) Scharfe, S.; Fässler, T. F. *Philos. Trans. R. Soc. London, Ser. A* **2010**, *368*, 1265−1284S. (b) Sevov, S. C.; Goicoechea, J. M. *Organometallics* **2006**, *25*, 5678−5692. (c) Moses, M. J.; Fettinger, J. C.; Eichhorn, B. W. *Science* **2003**, *300*, 778−780.
(6) Wang, J.-Q.; Stegmaier, S.; Wahl, B.; Fässler, T. F. *Chem.—Eur. J.* **2010**, *16*, 1793−1798.
(7) Esenturk, E. N.; Fettinger, J. C.; Eichhorn, B. W. *J. Am. Chem. Soc.* **2006**, *128*, 9178−9186.
(8) (a) Sun, Z.-M.; Xiao, H.; Li, J.; Wang, L.-S *J. Am. Chem. Soc.* **2007**, *129*, 9560−9561. (b) Kocak, F. S.; Zevalij, P.; Lam, Y.-F.; Eichhorn, B. W. *Inorg. Chem.* **2008**, *47*, 3515−3520.
(9) Goicoechea, J. M.; Sevov, S. C. *Angew. Chem.* **2005**, *117*, 4094−4096; *Angew. Chem., Int. Ed.* **2005**, *44*, 4026−4028.
(10) (a) Kumar, V.; Singh, A. K.; Kawazoe, Y. *Phys. Rev. B* **2006**, *74*, 125411−1−5. (b) Wang, J.; Han, J.-G. *J. Phys. Chem. B* **2006**, *110*, 7820−7827. (c) Ohara, M.; Miyajima, K.; Pramann, A.; Nakajima, A.; Kaya, K. *J. Phys. Chem. A* **2002**, *106*, 3702−3705.
(11) (a) Grubisic, A.; Ko, Y. J.; Wang, H.; Bowen, K. H. *J. Chem. Phys.* **2008**, *129*, 054302(1-5). (b) Grubisic, A.; Ko, Y. J; Wang, H.; Bowen, K. H. *J. Am. Chem. Soc.* **2009**, *131*, 10783−10790. (c) Dognon, J. P.; Clavaguéra, C.; Pyykkö, P. *Angew. Chem.* **2007**, *119*, 1449−1452; *Angew. Chem., Int. Ed.* **2007**, *46*, 1427−1430.
(12) Chen, S. W.; Lee, J. M.; Lu, K. T.; Pao, C. W.; Lee, J. F.; Chan, T. S.; Chen, J. M. *Appl. Phys. Lett.* **2010**, *97*, 012104−012107.
(13) Lips, F.; Clérac., R.; Dehnen, S. *Angew. Chem.* **2011**, *123*, 991−995; *Angew. Chem., Int. Ed.* **2011**, *50*, 960−964.
(14) [2.2.2]Crypt: 4,7,13,16,21,24-hexaoxa-1,10-diazabicyclo[8.8.8] hexacosane.
(15) Critchlow, S. C.; Corbett, J. D. *Inorg. Chem.* **1982**, *21*, 3286−3290.
(16) Sheldrick, G. M. SHELXTL 5.1, Bruker AXS Inc., 6300 Enterprise Lane, Madison, WI 53719−1173, USA, 1997.
(17) Absorption correction was applied using the program X-RED32 included in X-Area 1.54, STOE and Cie GmbH, Hilpertstraße 10, D64295 Darmstadt.
(18) TURBOMOLE V6.3, TURBOMOLE GmbH Karlsruhe, 2011, http://www.turbomole.de. TURBOMOLE is a development of University of Karlsruhe and Forschungszentrum Karlsruhe 1989-2007, TURBOMOLE GmbH since 2007.
(19) (a) Eichkorn, K.; Treutler, O.; Öhm, H.; Häser, M.; Ahlrichs, R. *Chem. Phys. Lett.* **1995**, *242*, 652−660. (b) Weigend, F. *Phys. Chem. Chem. Phys.* **2006**, *8*, 1057−1065.
(20) (a) Becke, A. D. *Phys. Rev. A* **1988**, *38*, 3098−3109. (b) Vosko, S. H.; Wilk, L.; Nusair, M. *Can. J. Phys.* **1980**, *58*, 1200−1205. (c) Perdew, J. P. *Phys. Rev. B* **1986**, *33*, 8822−8837.
(21) Weigend, F.; Ahlrichs, R. *Phys. Chem. Chem. Phys.* **2005**, *7*, 3297−3305.
(22) (a) Cao, X.; Dolg, M. *Molec. Struct. Theochem.* **2002**, *581*, 139−147. (b) Dolg, M.; Stoll, H.; Preuss, H. *J. Chem. Phys.* **1989**, *90*, 1730−1734.
(23) Dolg, M.; Stoll, H.; Savin, H.; Preuss, H. *Theor. Chim. Acta* **1989**, *75*, 173−194.
(24) Metz, B.; Stoll, H.; Dolg, M. *J. Chem. Phys.* **2000**, *113*, 2563−2569.
(25) (a) Klamt, A.; Schürmann, G. *J. Chem. Soc., Perkin Trans.* **1993**, *5*, 799−805. (b) Schäfer, A.; Klamt, A.; Sattel, D.; Lohrenz, J. C. W.; Eckert, F. *Phys. Chem. Chem. Phys.* **2000**, *2*, 2187−2193.
(26) (a) Lips, F.; Dehnen, S. *Angew. Chem.* **2009**, *121*, 6557−6560; *Angew. Chem., Int. Ed.* **2009**, *48*, 6435−6438. (b) Lips, F.; Dehnen, S. *Angew. Chem.* **2011**, *123*, 986−990; *Angew. Chem., Int. Ed.* **2011**, *50*, 955−959.
(27) Birchall, T.; Burns, R. C.; Devereux, L. A.; Schrobilgen, G. J. *Inorg. Chem.* **1985**, *24*, 890−894.
(28) Lippens, P. E. *Phys. Rev. B* **1999**, *60*, 4576−4586.
(29) Benelli, C.; Gatteschi, D. *Chem. Rev.* **2002**, *102*, 2369−2388.
(30) Sun, B.-Y.; Sugai, T.; Nishibori, E.; Iwata, K.; Sakata, M.; Takata, M.; Shinohara, H. *Angew. Chem.* **2005**, *117*, 4644−4647; *Angew. Chem., Int. Ed.* **2005**, *44*, 4568−4571.
(31) (a) Zintl, E. *Angew. Chem.* **1939**, *52*, 1−6. (b) Klemm, W. *Proc. Chem. Soc. London* **1959**, 329−341. (c) Busmann, E. *Z. Allg. Anorg. Chem.* **1961**, *313*, 90−106. (d) Kauzlarich, S. M. Ed. *Chemistry, Structure and Bonding of Zintl Phases and Ions*; VCH: New York, 1996.
(32) Frank, F. C.; Kasper, J. S. *Acta Crystallogr.* **1958**, *11*, 184−190.

(33) Deng, L.; Chan, H.-S.; Xie, Z. *Angew. Chem.* **2005**, *117*, 2166−2169; *Angew. Chem., Int. Ed.* **2005**, *44*, 2128−2131.
(34) Köhnlein, H.; Stößer, G.; Baum, E.; Möllhausen, E.; Huniar, U.; Schnöckel, H. *Angew. Chem.* **2000**, *112*, 827−830; *Angew. Chem., Int. Ed.* **2000**, *39*, 799−801.
(35) Wilson, N. M. M.; Ellis, D.; Boyd, A. S. F.; Giles, B. T.; Macgregor, S. A.; Rosair, G. M.; Welch, A. J. *Chem. Commun.* **2002**, 464−465.
(36) Burke, A.; Ellis, D.; Giles, B. T.; Hodson, B. E.; Macgregor, S. A.; Rosair, G. M.; Welch, A. J. *Angew. Chem.* **2003**, *115*, 235−238; *Angew. Chem., Int. Ed.* **2002**, *42*, 225−228.
(37) Komura, Y.; Tokunaga, K. *Acta Crystallogr., Sect. B* **1980**, *36*, 1548−1554.
(38) (a) Bichara, C.; Pellegatti, A.; Gaspard, J.-P. *Phys. Rev. B* **1993**, *47*, 5002−5007. (b) Sheng, H. W.; Luo, W. K.; Alamgir, F. M.; Bai, J. M.; Ma, E. *Nature* **2006**, *439*, 419−425.
(39) Heath, J.; O'Brien, S. C.; Zhang, Q.; Liu, Y.; Curl, R. F.; Kroto, H. W.; Tittel, F. K.; Smalley, R. E. *J. Am. Chem. Soc.* **1985**, *107*, 7779−7780.
(40) Cadenbach, T.; Bollermann, T.; Gemel, C.; Tombul, M.; Fernandez, I.; von Hopffgarten, M.; Frenking, G.; Fischer, R. A. *J. Am. Chem. Soc.* **2009**, *131*, 16063−16077. (b) Cadenbach, T.; Bollermann, T.; Gemel, C.; Fernandez, I.; von Hopffgarten, M.; Frenking, G.; Fischer, R. A. *Angew. Chem.* **2008**, *120*, 9290−9295; *Angew. Chem., Int. Ed.* **2008**, *47*, 9150−9154.
(41) Esenturk, E. N.; Fettinger, J.; Eichhorn, B. *Chem. Commun.* **2005**, 247−249.
(42) (a) Wang, J.-Q.; Stegmaier, S.; Fässler, T. F. *Angew. Chem.* **2009**, *121*, 2032−2036; *Angew. Chem., Int. Ed.* **2009**, *48*, 1998−2002. (b) Zhou, B.; Denning, M. S.; Kays, D. L.; Goicoechea, J. M. *J. Am. Chem. Soc.* **2009**, *131*, 2802−2803.
(43) Kerr, J. A., Stocker, D. W., Lide D. R., Eds. *CRC Handbook of Chemistry and Physics*, 81st ed.; CRC Press: Boca Raton, FL, 2001; pp 952−957.
(44) Kummer, D.; Diehl, L. *Angew. Chem.* **1970**, *82*, 881−882; *Angew. Chem., Int. Ed.* **1970**, *9*, 895−896. (b) Critchlow, S. C.; Corbett, J. D. *J. Am. Chem. Soc.* **1983**, *105*, 5715−5716.
(45) (a) Wade, K. *Adv. Inorg. Radiochem.* **1976**, *18*, 1−66. (b) Mingos, D. M. P. *Nat. Phys. Sci.* **1972**, *236*, 99−102. (c) Mingos, D. M. P. *Acc. Chem. Res.* **1984**, *17*, 311−319.
(46) (a) Boys, S. F. *Rev. Mod. Phys.* **1960**, *32*, 296−299. (b) Foster, J. M.; Boys, S. F. *Rev. Mod. Phys.* **1960**, *32*, 300−302.
(47) Pipek, J.; Mezey, P. G. *J. Chem. Phys.* **1989**, *90*, 4916−4926.
(48) Mulliken, R. S. *J. Chem. Phys.* **1955**, *23*, 1833−1840.
(49) Wei, H.; Wu, Y.; Lun, N.; Zhao, F. *J. Mater. Sci.* **2004**, *39*, 1305−1308.